National Conference on Applied Sciences Synergising the Engineering and Technology
Print ISSN: 2395-6011 | Online ISSN: 2395-602X (www.ijsrst.com)
© 2021 IJSRST | Volume 8 | Issue 2

Hirshfeld Surface Analysis and DFT Calculations of 2-Amino-N-(2-Fluorophenyl)-4,5,6,7-Tetrahydro-1-Benzothiophene-3-Carboxamide

Madhura TK[1], Rajesh BM[2], Chandra Kumar K[3], Shubha S[2], Chandra[4]

[1]Department of Physics, Mount Carmel College, Autonomous, Bengaluru, Karnataka, India

[2]Department of Physics, RV College of Engineering, Bengaluru, Karnataka, India

[3]Department of Engineering, Physics HKBK College of Engineering, Bengaluru, Karnataka, India

[4]Department of Physics, The National Institute of Engineering, Mysore, Karnataka, India

ABSTRACT

Thiophene nucleus has been established as a potential entity in the heterocyclic compounds possessing promising pharmacological characteristics such as anti-HIV PR inhibitors and anti-breast cancer activities. Importantly, benzothiophene derivative shows significant antimicrobial and anti-inflammatory activities. The title compound, $C_{15}H_{15}FN_2OS$ was characterized by single-crystal X-ray diffraction studies. The molecular conformation is consolidated by intramolecular N-H···F and N-H···O hydrogen bonds. The Hirshfeld surface analysis revealed that H···H and C···H contacts contribute significantly to the intermolecular interactions. Further, their structures were optimized by density functional theory (DFT) calculations using B3LYP hybrid functionals with 6-31G(d,p) level basis set. The transitions among the molecular orbital's were investigated using time-dependent density functional theory (TD-DFT) and the UV–Vis spectra showed the absorption peak at 306 nm. In addition, natural bond orbital (NBO) analysis was carried out to explore inter/intra molecular electron delocalization and hyperconjugative interactions responsible for the molecular structure stability.

Keywords - Hirshfeld, DFT and Thiophene

I. INTRODUCTION

Thiophene and its substituted derivatives are very important entity in the heterocyclic compounds shows a promising pharmacological characteristics. It possess various biological activities such as anti-bacterial, anti-inflammatory, anti-depressive, analgesic, anti-allergic, anti-fungal, antibacterial, anti-microbial and anti-cancer activities [1]. Due to its importance, the 2-amino-N-(2-fluorophenyl)- 4,5,6,7-tetrahydro-1-benzothiophene-3-carboxamide was synthesized and the molecular structure was studied using a X-ray diffraction method. The single crystal XRD analysis reveals that the title compound $C_{15}H_{15}FN_2OS$ crystallizes in the monoclinic system in Cc space group with the unit cell parameter a= 11.213 Å, b= 14.231 Å, c= 09.582 Å, $\alpha = 90°$, $\beta = 116.76°$ and $\gamma = 90°$, Z=4, V = 1365 $Å^3$ [2]. In addition, the combination between benzothiophene and other ring molecule was used in different pharmaceutical applications and the theoretical study on molecular geometry, vibrational,

pharmaceutical and electronic properties were carried out using DFT B3LYP hybrid functional [3]. Hirshfeld surface analysis was used to study intermolecular interactions in the heterocyclic compound [4].

II. COMPUTATIONAL METHOD

A. Hirshfeld SurfaceAnalysis

The Crystal Explorer 17.5 tool is used to perform Hirshfeld surface (HS) analysis to understand the intermolecular interactions and packing modes of the title compound $C_{15}H_{15}FN_2OS$ [5]. The CIF file data (CCDC No-1045467) obtained from the XRD measurements was used for performing the calculations. To quantify the intermolecular contacts present within the crystal structure of the compound, the HS and fingerprint plots were generated and analyzed. The contact distances d_{norm} is based on d_e and d_i, where d_e represents the distance between a point on the surface to the nearest nucleus outside the surface and d_i the distance between a point on the surface to the nearest nucleus inside the surface and it is calculated using the formula,

$$d_{norm} = \frac{d_i - r_i^{vdW}}{r_i^{vdW}} + \frac{d_e - r_e^{vdW}}{r_e^{vdW}}$$

Where, r_e^{vdW} and r_i^{vdW} are the vander Waal radii of the nearest nucleus outside and inside the surface.

B. DFT calculations

To understand the frontier molecular orbital energies of the compound $C_{15}H_{15}FN_2OS$, the structure is optimized by the Gaussian 16 package using the density functional theory (DFT) method with the basis set of B3LYP/6-31G(d,p) based on the single-crystal X-ray diffraction structure data (CCDC reference: 1045467) [6]. Comparative analysis of theoretically computed data with experimental data of the studied compound is obtained for better description. In addition, vibrational frequency calculations were conducted to get IR frequencies. Electronic properties such as energy of highest occupied molecular orbital (E_{HOMO}), lowest unoccupied molecular orbital (E_{LUMO}) and (E_{gap}) energy gap between HOMO and LUMO is measured with the visual representation is shown in fig. 8.

III. RESULTS AND DISCUSSION

A. Hirshfeld surface analysis

Hirshfeld Surface indicating d_{norm}, Shape index, Fragment patch and Curvdness of title compound $C_{15}H_{15}FN_2OS$ is as shown in the fig.1. The red spots indicate the strong intermolecular interactions with negative d_{norm} value where as light red spots shows the weak interactions. The blue regions correspond to longer contacts with positive d_{norm} value. A white region represents the distance of contact exactly equal to Van der Waal separation with a d_{norm} value of zero. The shape of electron density and surface around the molecular interactions is represented by shape index. The curvedness is a measure of the shape of the surface area of the molecule.

The 2D fingerprint plots of the title compound is as shown in fig. 2, highlighting the H...H contributing 47.3% of the overall crystal packing which has large hydrogen content of the molecule with the tip at 1.18Å, H...S contributing 10.8% having pair of spikes with tips at d_e+d_i =~2.9Å, H...C contributing 16.3% having pair of wings with one edge at d_e+d_i =~ 2.8Å and another at d_e+d_i =~ 23.42Å. These interactions are the primary contributors to the intermolecular stabilization in the crystal as shown in the fig.3 [7]. From the total contributions the H···H contacts has maximum and F···S has minimum contributions. Similarly the H-S, H-F, H-O, H-N, H-C, O-C, C-C, C-N, C-F, C-S and N-F contacts also contribute to the total area of the surface. The red and blue triangular patches on the same region of the shape index shows the π-π stacking [8]. Curvedness is a function of the root-mean-square curvature of the surface showing the flat areas having lower curvedness and sharp curvature having high curvedness. The calculated volume inside the Hirshfeld surface is 334.99 Å3 in the area of 307.19 Å2 with globularity (G) 0.759 as well as asphericity (U) 0.202. The overall calculation is performed with the Gaussian 16 integrated with Crystal Explorer.

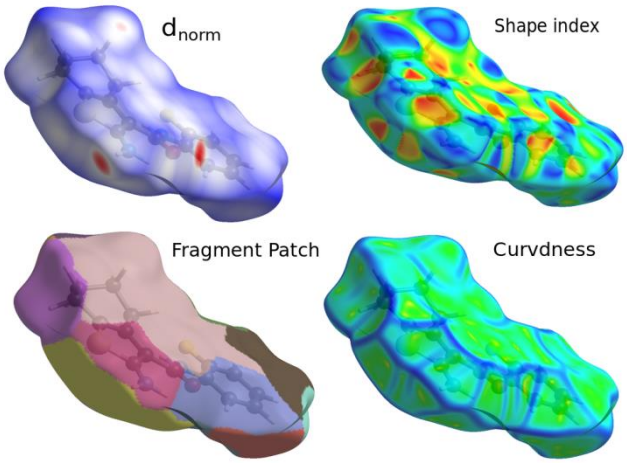

Fig. 1. Hirshfeld Surface d_{norm}, Shape index, Fragment patch and Curvdness of $C_{15}H_{15}FN_2OS$

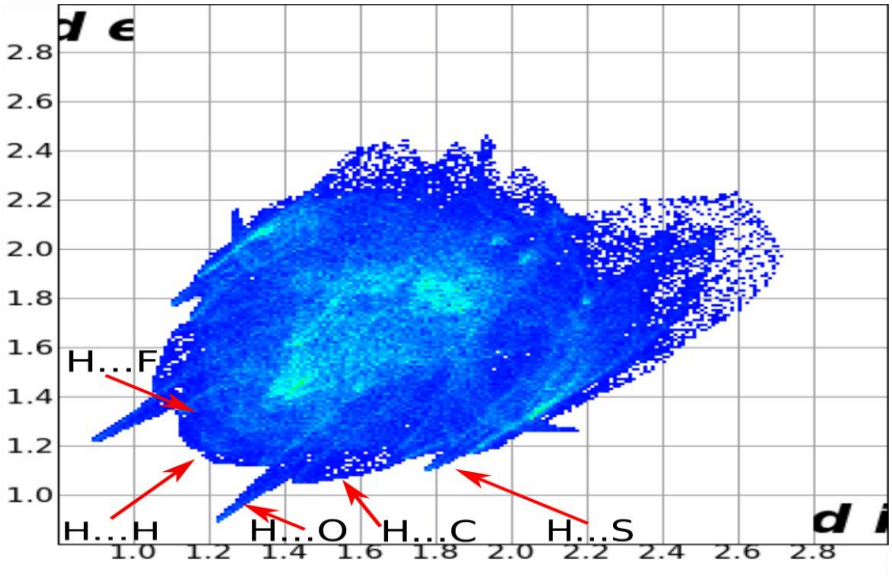

Fig. 2. The 2D fingerprint plot showing overall crystal packing.

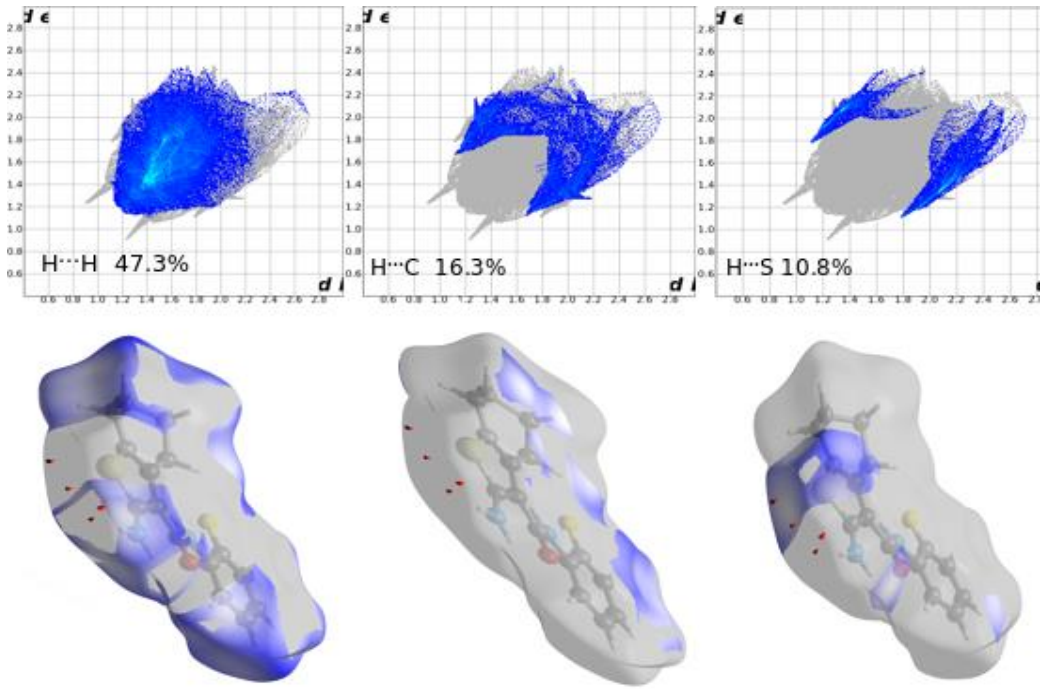

Fig. 3. The 2D fingerprint plots of H…H, H…C and H…S interactions with Hirshfeld surface.

Molecular electrostatic potential is used to visualize the active sites and the relative polarity of the molecule as shown in the fig. 4. The negative potential, red region is located over the terminal oxygen of the molecule.

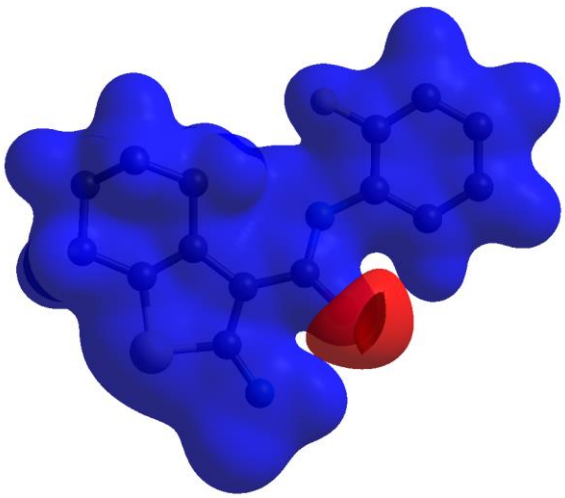

Fig. 4. Electrostatic Potential map of the molecule range 0.0500 to 0.0500 a.u. using the B3LYP/6-31G(d,p) Gaussian basis set at the DFT level of theory.

Interaction energy calculations:

The intermolecular interaction energies were calculated using the B3LYP/6–31G(d,p) basis set energy model in Crystal Explorer 17.5 [9], where a cluster of molecules is generated by applying crystallographic symmetry operations with respect to a selected central molecule within a default radius of 3.8 Å is as shown in fig. 5 [10]. The total intermolecular energy (E_{tot}) is the sum of electrostatic (E_{ele}), polarization (E_{pol}), dispersion (E_{dis}) and exchange-repulsion (E_{rep}) energies [11] with scale factors of 1.057, 0.740, 0.871 and 0.618, respectively.

Hydrogen bonding interaction energies (in kJ mol^{-1}) were calculated as -9.8(E_{ele}), -3.1 (E_{pol}), -64.2 (E_{dis}), 34.1 (E_{rep}) and -47.5 (E_{tot}) is tabulated in table 1.

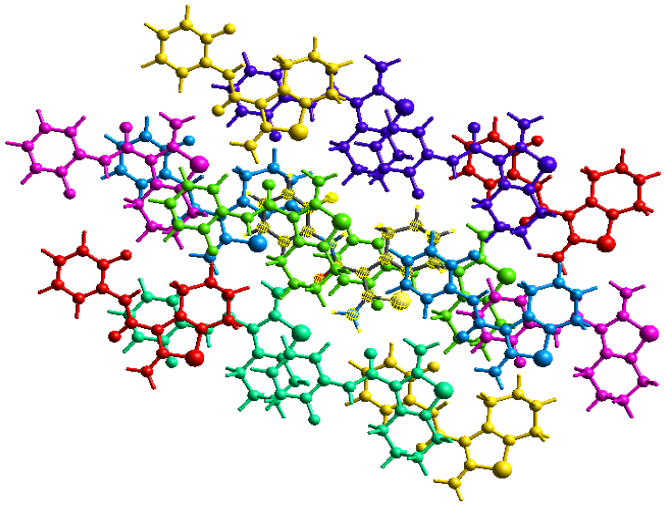

Fig. 5. Interaction energies for a 3.8Å cluster around the selected fragment.

TABLE 1: ENERGY FRAMEWORK DETAIL OF INTERACTION WITH COLOUR-CODED SYMMETRY OPERATIONS (SYMMOP) AND DISTANCES BETWEEN MOLECULAR CENTROIDS (R) IN Å.

	N	Symmop	R	Electron Density	E_{ele}	E_{pol}	E_{dis}	E_{rep}	E_{tot}
	2	x+1/2, y+1/2, z	11.20	B3LYP/6-31G(d,p)	-0.8	-0.1	-6.1	1.4	-5.4
	2	x+1/2, y+1/2, z	11.20	B3LYP/6-31G(d,p)	-2.7	-1.3	-10.5	6.8	-8.7
	2	x+1/2, -y+1/2, z+1/2	5.50	B3LYP/6-31G(d,p)	-9.8	-3.1	-64.2	34.1	-47.5
	2	x, -y, z+1/2	8.69	B3LYP/6-31G(d,p)	-24.9	-4.9	-17.7	26.4	-29.0
	2	x, y, z	9.58	B3LYP/6-31G(d,p)	-2.5	-0.9	-22.2	11.0	-15.8
	2	x, -y, z+1/2	8.47	B3LYP/6-31G(d,p)	-3.4	-0.5	-24.1	12.5	-17.2
	2	x+1/2, -y+1/2, z+1/2	12.86	B3LYP/6-31G(d,p)	-1.6	-0.2	-11.3	7.7	-6.9

B. DFT calculations

Geometry optimization of the compound

The optimized structure and its atoms numbering with Milliken charges are displayed in Fig. 6. The optimized geometry is correlated with the crystallographic data of the title compound and the correlation coefficient of 0.969 and 0.952 for bond length and the bond angles respectively is tabulated in the table 2 and 3. The overall energy minimum of 2-amino-N-(2-fluorophenyl)-4,5,6,7-tetrahydro-1-benzothiophene-3-carboxamide is -1263.44 Hartree with Dipole moment (μ)1.6989 Debye as calculated with B3LYP/6-31G(d,p) basis set. The optimization studies shows that the molecule be appropriate to C_1 symmetry point group.

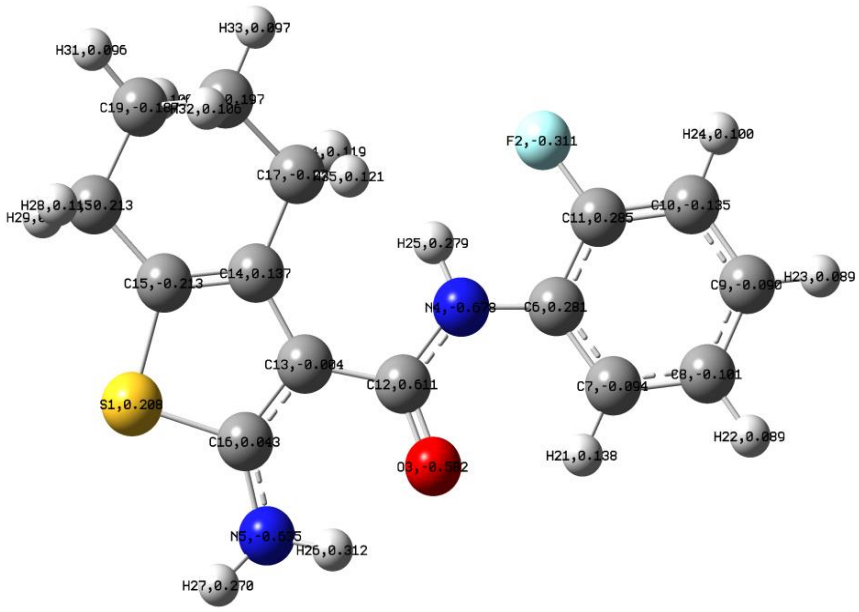

Fig. 6. Optimized structure with Mulliken charges.

Spectroscopic measurement

UV-visible spectrum analysis

Theoretical UV-visible spectrum calculation has been carried out to have better understanding of charge delocalization pattern, electron densities of the atoms, electron transition and stability of the title molecule [12]. In the present study, the maximum absorption wavelengths (λ_{max}), excitation energies (ΔE) and oscillator strengths (f) of the title molecule in the gaseous phase are computed using the TD DFT/B3YLP/6-31G(d,p) basis set level. The simulated UV-visible spectrum of the title molecule is shown in fig. 7 and the molecule have three maximum absorption peaks at 263.4, 284.9 and 306.9 nm with oscillator strengths 0.0288, 0.0038 and 0.2292 a.u respectively. The observed peaks in the spectrum are due to one electron excitation from HOMO-LUMO (ΔE=0.164 eV) is shown in fig. 8, HOMO-1-LUMO (ΔE=0.194 eV) and HOMO-2-LUMO (ΔE=0.221 eV).

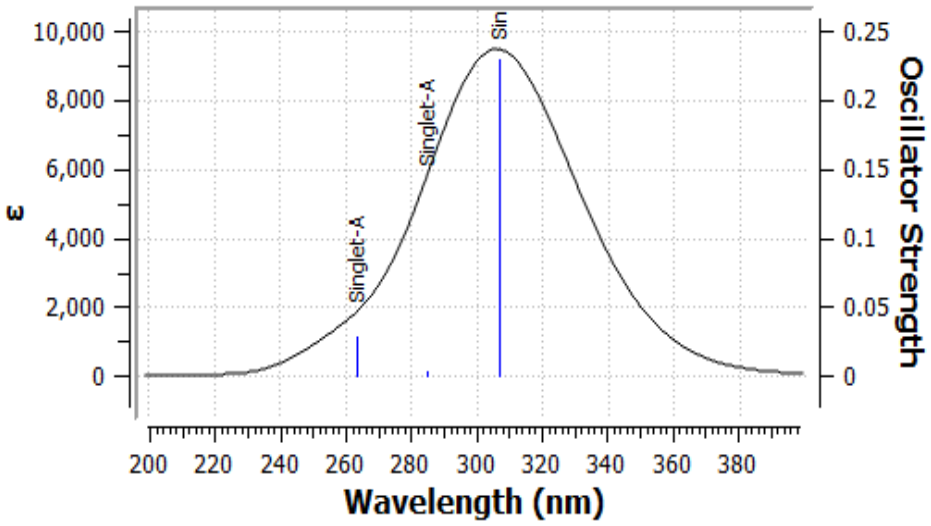

Fig. 7. UV-visible spectrum

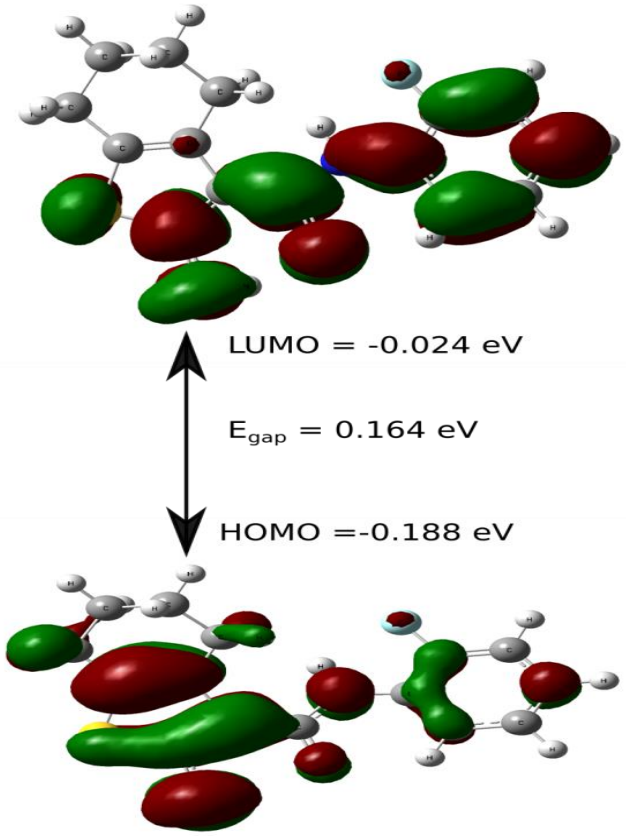

Fig. 8. HOMO, LUMO and E_{gap} of the title molecule.

IR Spectrum analysis

Theoretically calculated IR spectrum is as shown in fi. 9. In the IR spectrum the strong absorption band at 3478 cm^{-1} indicates the presence of amide NH and two peaks at 3666, 3690 cm^{-1} for the presence of amide NH^2 group. Peak at 1635 cm^{-1} shows the C=O stretching.

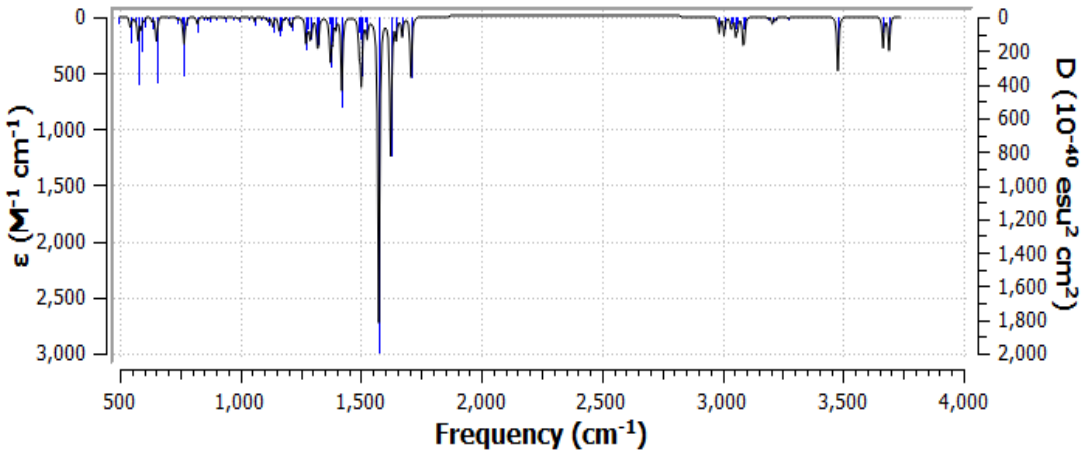

Fig. 9. IR spectrum

The electrostatic potential of the crystal can be analysed by obtaining the positive and negative charge distribution. This Molecular Electrostatic potential (MEP) from -4.68×10^{-2} to 4.68×10^{-2} is obtained using B3LYP/6-31G(d,p). In fig.10 the red colour indicates is the maximum negative region providing the site for electrophilic attack and the blue colour indicates maximum positive region providing the site for nucleophilic

attack. This MEP map shows that there is electrophilic site localised at O(3) atom and nucleophilic site located at H(27). This shows that the most reactive site of the molecule is the site containing the oxygen [13].

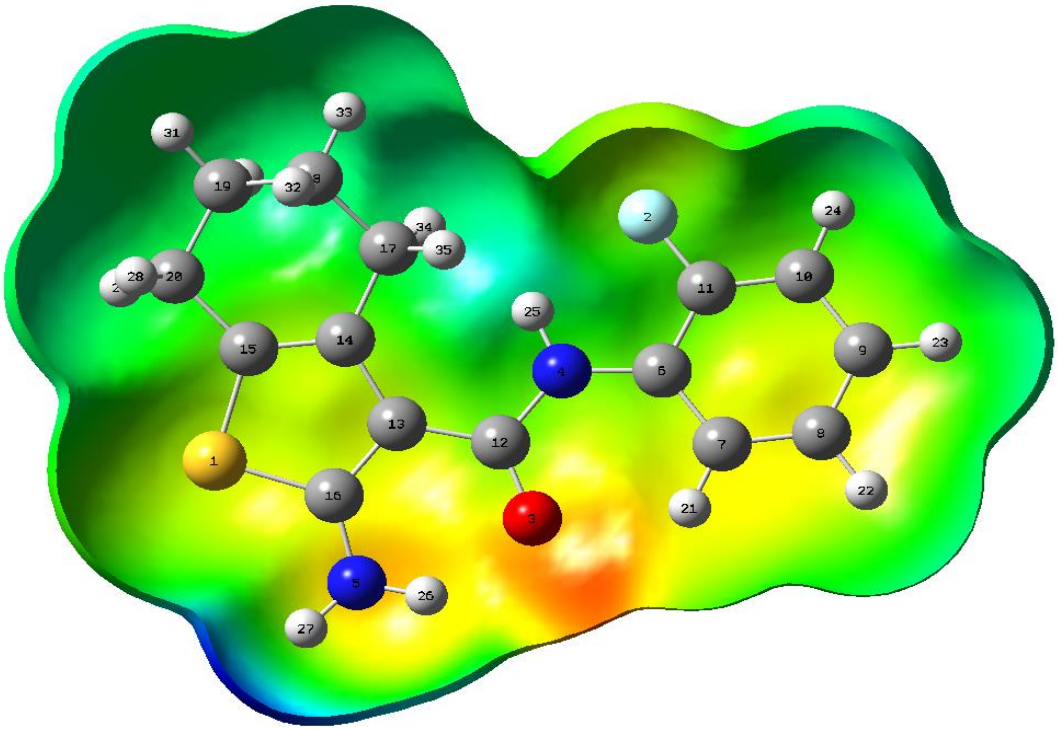

Fig. 10. 3D-representation of the electrostatic potential around the molecule using the Density Functional Theory at B3LYP level of theory at 6-31G(d,p).

Natural Bond Orbital Analysis

The most possible accurate "natural Lewis structure" is obtained by natural bond orbital (NBO) analysis. It gives the information about interactions in both filled and virtual orbital spaces enhancing the possible intra and intermolecular hydrogen bond. With the help of NBO, shifting of charges from the filled bonding molecular orbital to empty non bonding molecular orbital can easily be indicated. The following equation gives stabilization energy (electronic delocalization). In the given equation, q_i is orbital occupancy, ε_i and ε_j are diagonal NBO Fock matrix elements and f_{ij} is off diagonal NBO Fock matrix element respectively [14].

$$E^2 = q_i \frac{f_{ij}^2}{\varepsilon_j - \varepsilon_i}$$

IV. REFERENCES

[1]. B. Pramodh, K. C. Prathap, M. Hema, I. Warad, and N. Lokanath, "Synthesis, structure, quantum computational and biological studies of novel thiophene derivatives," Journal of Molecular Structure, p. 129587, 2020.

[2]. K. Chandra Kumar, V. Umesh, T. Madhura, B. Rajesh, and Chandra, "Crystal structure of 2-amino-N-(2-fluorophenyl)-4, 5, 6, 7-tetrahydro-1-benzothiophene-3-carboxamide," Acta Crystallographica Section E: Crystallographic Communications, vol. 71, pp. o807-o808, 2015.

[3]. A. Sagaama and N. Issaoui, "Design, molecular docking analysis of an anti-inflammatory drug, computational analysis and intermolecular interactions energy studies of 1-benzothiophene-2-carboxylic acid," Computational biology and chemistry, vol. 88, p. 107348, 2020.

[4]. A. V. Ivachtchenko, O. D. Mitkin, D. V. Kravchenko, S. M. Kovalenko, S. V. Shishkina, N. D. Bunyatyan, I. S. Konovalova, I. G. Dmitrieva, V. V. Ivanov, and T. Langer, "Synthesis, X-ray crystal structure, Hirshfeld surface analysis, and molecular docking study of novel inhibitor of hepatitis B: Methyl 4-fluoro-3-(morpholinosulfonyl) benzo b] thiophene-2-carboxylate," Heliyon, vol. 5, p. e02738, 2019.

[5]. M. A. Spackman and D. Jayatilaka, "Hirshfeld surface analysis," CrystEngComm, vol. 11, pp. 19-32, 2009.

[6]. M. Frisch, "Gaussian 09 Revision D. 01; b) MJ Frisch, GW Trucks, HB Schlegel, GE Scuseria, MA Robb, JR Cheeseman, G. Scalmani, V. Barone, GA Petersson, H. Nakatsuji et al," Gaussian 16 Revision A, vol. 3, 2016.

[7]. L. H. Al-Wahaibi, J. Joubert, O. Blacque, N. H. Al-Shaalan, and A. A. El-Emam, "Crystal structure, Hirshfeld surface analysis and DFT studies of 5-(adamantan-1-yl)-3-(4-chlorobenzyl) sulfanyl]-4-methyl-4 H-1, 2, 4-triazole, a potential 11β-HSD1 inhibitor," Scientific reports, vol. 9, pp. 1-11, 2019.

[8]. K. Azouzi, B. Hamdi, R. Zouari, and A. B. Salah, "Synthesis, structure and Hirshfeld surface analysis, vibrational and DFT investigation of (4-pyridine carboxylic acid) tetrachlorocuprate (II) monohydrate," Bulletin of Materials Science, vol. 40, pp. 289-299, 2017.

[9]. M. Turner, J. McKinnon, S. Wolff, D. Grimwood, P. Spackman, D. Jayatilaka, and M. Spackman, "CrystalExplorer17; University of Western Australia: Crawley, Australia, 2017," Google Scholar There is no corresponding record for this reference, 2017.

[10]. M. J. Turner, S. Grabowsky, D. Jayatilaka, and M. A. Spackman, "Accurate and efficient model energies for exploring intermolecular interactions in molecular crystals," The journal of physical chemistry letters, vol. 5, pp. 4249-4255, 2014.

[11]. M. J. Turner, S. P. Thomas, M. W. Shi, D. Jayatilaka, and M. A. Spackman, "Energy frameworks: insights into interaction anisotropy and the mechanical properties of molecular crystals," Chemical Communications, vol. 51, pp. 3735-3738, 2015.

[12]. V. Balachandran, T. Karthick, S. Perumal, and A. Nataraj, "Comparative theoretical studies on natural atomic orbitals, natural bond orbitals and simulated UV-visible spectra of N-(methyl) phthalimide and N-(2 bromoethyl) phthalimide," 2013.

[13]. R. Rahmani, N. Boukabcha, A. Chouaih, F. Hamzaoui, and S. Goumri-Said, "On the molecular structure, vibrational spectra, HOMO-LUMO, molecular electrostatic potential, UV–Vis, first order hyperpolarizability, and thermodynamic investigations of 3-(4-chlorophenyl)-1-(1yridine-3-yl) prop-2-en-1-one by quantum chemistry calculations," Journal of Molecular Structure, vol. 1155, pp. 484-495, 2018.

[14]. M. Khalid, M. N. Arshad, M. N. Tahir, A. M. Asiri, M. M. Naseer, M. Ishaq, M. U. Khan, and Z. Shafiq, "An efficient synthesis, structural (SC-XRD) and spectroscopic (FTIR, 1HNMR, MS spectroscopic) characterization of novel benzofuran-based hydrazones: An experimental and theoretical studies," Journal of Molecular Structure, vol. 1216, p. 128318, 2020.

TABLE 2: BOND ANGLES FROM X-RAY CRYSTALLOGRAPHY AND USING B3LYP/6-31G(D,P) BASIS SET

Atom1	Exp (X-ray)	B3LYP	Atom	Exp (X-ray)	B3LYP
C15-S1-C16	91.9(1)	91.5	C11-C12-C17	127.1(2)	126.75
C1-N8-C9	129.3(2)	128.49	C13-C12-C17	119.3(3)	119.78
C1-N8-H9A	115.3	113.74	S14-C13-C12	111.6(2)	111.73
C9-N8-H9A	115.4	117.67	S14-C13-C20	120.3(2)	120.95
C15-N16-H15C	120	113.12	C12-C13-C20	128.1(3)	127.3
C15-N16-H15D	120.1	119.1	S14-C15-N16	118.8(2)	120.52
H15C-N16-H15D	119.9	119.31	S14-C15-C11	111.5(2)	111.8
N8-C1-C2	125.8(2)	126.4	N16-C15-C11	129.6(3)	127.6
N8-C1-C6	117.1(2)	116.27	C12-C17-C18	111.9(2)	112.44
C2-C1-C6	117.1(3)	117.33	C12-C17-H22A	109.2	110.11
C1-C2-C3	119.9(3)	119.86	C12-C17-H22B	109.2	110.31
C1-C2-H2A	120	118.66	C18-C17-H22A	109.3	108.62
C3-C2-H2A	120.1	121.47	C18-C17-H22B	109.3	108.63
C2-C3-C4	121.0(3)	121.42	H22A-C17-H22B	107.9	106.54
C2-C3-H3A	119.5	118.74	C17-C18-C19	111.7(2)	111.68
C4-C3-H3A	119.5	119.84	C17-C18-H21A	109.3	109.1
C3-C4-C5	119.8(3)	119.45	C17-C18-H21B	109.3	109.32
C3-C4-H4A	120.1	120.69	C19-C18-H21A	109.3	109.13
C5-C4-H4A	120.1	119.86	C19-C18-H21B	109.3	110.71
C4-C5-C6	118.6(3)	118.57	H21A-C18-H21B	107.9	106.78
C4-C5-H5A	120.6	122.33	C18-C19-C20	112.1(3)	110.52
C6-C5-H5A	120.8	119.1	C18-C19-H20A	109.1	109.43
F7-C6-C1	117.0(2)	117.14	C18-C19-H20B	109.1	110.63
F7-C6-C5	119.4(3)	119.5	C20-C19-H20A	109.2	109.43
C1-C6-C5	123.6(3)	123.36	C20-C19-H20B	109.2	109.8
O10-C9-N8	120.4(3)	120.77	H20A-C19-H20B	107.9	106.96
O10-C9-C11	122.8(3)	122.12	C13-C20-C19	109.8(2)	109.99
N8-C9-C11	116.8(2)	117.11	C13-C20-H18A	109.7	110.28
C9-C11-C12	129.8(2)	130.31	C13-C20-H18B	109.8	110.65
C9-C11-C15	118.7(2)	118.18	C19-C20-H18A	109.7	109.68
C12-C11-C15	111.5(2)	111.5	C19-C20-H18B	109.7	110.1
C11-C12-C13	113.5(3)	113.44	H18A-C20-H18B	108.2	106.07

TABLE 3: BOND LENGTHS FROM CALCULATIONS USING X-RAY CRYSTALLOGRAPHY AND B3LYP/6-31G(D,P) BASIS SET

Atom	Exp (X-ray)	B3LYP	Atom	Exp (X-ray)	B3LYP	Atom	Exp (X-ray)	B3LYP
S14-C13	1.749(3)	1.7631	C2-C3	1.387(5)	1.3966	C13-C20	1.497(4)	1.503
S14-C15	1.734(4)	1.7495	C2-H2A	0.93	1.0797	C17-C18	1.530(4)	1.539
F7-C6	1.357(3)	1.3643	C3-C4	1.382(6)	1.3943	C17-H22A	0.97	1.102
O10-C9	1.238(3)	1.2428	C3-H3A	0.93	1.0857	C17-H22B	0.969	1.0964
N8-C1	1.400(4)	1.4014	C4-C5	1.370(5)	1.3974	C18-C19	1.505(6)	1.5321
N8-C9	1.377(3)	1.3809	C4-H4A	0.93	1.0851	C18-H21A	0.97	1.0976
N8-H9A	0.859	1.0073	C5-H5A	0.929	1.0845	C18-H21B	0.97	1.0953
N16-C15	1.350(4)	1.3587	C9-C11	1.449(4)	1.4723	C19-C20	1.525(4)	1.5372
N16-H15C	0.861	1.0178	C11-C12	1.460(4)	1.461	C19-H20A	0.97	1.0976
N16-H15D	0.86	1.0076	C11-C15	1.387(4)	1.3977	C19-H20B	0.97	1.0954
C1-C2	1.386(4)	1.4034	C12-C13	1.346(4)	1.3624	C20-H18A	0.971	1.1002
C1-C6	1.388(4)	1.4041	C12-C17	1.516(4)	1.5169	C20-H18B	0.97	1.0972